Appl. Phys. B 73, 687–692 (2001)
DOI: 10.1007/s003400100734

Applied Physics B
Lasers and Optics

N.A. PAPADOGIANNIS[1,2,✉]
C. KALPOUZOS[1]
E. GOULIELMAKIS[1,2]
G. NERSISYAN[1,3]
D. CHARALAMBIDIS[1,2]
F. AUGÉ[4]
F. WEIHE[4]
PH. BALCOU[4]

Kilohertz extreme-ultraviolet light source based on femtosecond high-order harmonic generation from noble gases

[1] Foundation for Research and Technology-Hellas, Institute of Electronic Structure and Laser, Laser and Applications Division, P.O. Box 1527, 71110 Heraklion, Crete, Greece
[2] Physics Department, University of Crete, Heraklion, Crete, Greece
[3] Institute for Physical Research, NAS, Ashtarak-2, 378410, Armenia
[4] Laboratoire d'Optique Appliquée, ENSTA-Ecole Polytechnique, Unité Mixte de Recherches 7639, Centre National de la Recherche Scientifique, 91761 Palaiseau Cedex, France

Received: 9 July 2001/Revised version: 1 August 2001
Published online: 7 November 2001 •

ABSTRACT A compact, versatile table-top kilohertz source of coherent extreme-ultraviolet (XUV) radiation in the wavelength region 18–100 nm, based on high-order harmonic generation from noble gases induced by a 40-femtosecond Ti:sapphire laser system, is presented. The XUV beamline delivers at its output 10^8 photons/s at a wavelength of 23 nm. The monochromatized XUV radiation is directly focused onto a 10^{-2}-mm^2 spot by a toroidal grating, allowing one to reach intensities higher than 10^6 W/cm^2. Optimization results are presented for a new XUV-generating geometry, utilizing a 'semi-infinite' quasi-static gas cell and strong focusing. In those conditions, we observe an anomalous inversion between the cutoffs of argon and krypton, with the krypton spectrum extending to much higher orders than expected in an adiabatic limit.

PACS 42.65.Ky; 32.80.Rm; 42.50.Hz

1 Introduction

The phenomenon of high-order harmonic generation (HHG) in gases has been studied for several years, not only because of the fundamental interest in the behavior of atoms under the influence of the intense laser field but also for two additional reasons: covering the need for table-top tunable coherent radiation sources in the extreme-ultraviolet (XUV) region and its prospects towards attosecond pulse generation.

Several facets of the physics involved in the HHG towards the realization of the above-mentioned targets have been elucidated. Mixing of an ultraviolet laser with a tunable infrared laser leads to the generation of tunable harmonics in the extreme-ultraviolet region [1–3]. Enhancement of HHG has been achieved by using ultra-fast laser drivers [4, 5], phase phenomena [6–10], femtosecond light guiding in waveguides [11–13] and self-guiding in ionized gases [12, 13]. Other related works deal with the harmonic characterization: pulse-duration measurements [14–16], spatial and temporal coherence [17–19], polarization and laser ellipticity dependence [20–24], geometric characteristics [25] and spectral profiles [26–30]. Further reports have dealt with the generation and measurement of pulses of less than 1-fs duration [31–41] and the usage of the high-order harmonics [42, 43].

In the present work a novel geometry for a XUV source, based on 1-kHz high-order harmonic generation of ultra-short Ti:sapphire pulses in rare-gas targets, is developed, tested, opt imized and used for spectroscopic studies. For the sake of compactness and simplicity, we use (i) strong laser focusing, so that vacuum intensities may approach 10^{15} W/cm^2, and (ii) a 'semi-infinite' cell, for which the laser beam propagates into the noble gas from the focusing lens up an exit pinhole close to the focus. We present quantitative measurements of the XUV photons produced in a large spectral range based on calibrated diodes. It should be noted here that throughout the paper we specify the number of photons at the exit slit of the source rather than the number of photons generated, because the former is the relevant usable quantity of a light source and does not require vague corrections. The performance of the source at different experimental parameters is investigated and discussed here. In particular, we report an anomalous extent of the plateau of high harmonics in Kr, with a cutoff at wavelengths shorter than for the Ar cutoff. Pressure and focus-position dependences, as well as spectral structures within each harmonic, are also discussed.

2 Experimental set-up

The source consists of three main units: (a) the XUV-generation unit, (b) the monochromatization and focusing unit and (c) the detection and calibration unit.

2.1 *Generation of XUV radiation*

The generation of the XUV pulses is based on the effect of high-order harmonic generation in noble gases, induced by 1-kHz Ti:sapphire lasers with a pulse duration of the order of 50 fs. The energies used range from 0.25 to 2.4 mJ. The use of the conventional geometry of gas injection in a vacuum chamber through pulsed nozzle valves and the focus of the laser beam in the cone of the injected gas is not straightforward at a kHz laser repetition rate. For this reason several other geometries have been tested prior to the construction of the source, such as continuous gas nozzles (hollow capillaries with a pinhole gas output diameter of the order of 50 μm), microcells forming a thin gas layer as well as quasi-static cells

✉ Fax: +30-81/391-318, E-mail: papadogi@iesl.forth.gr

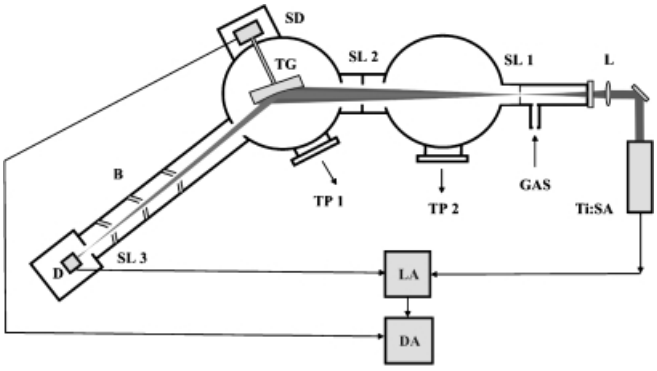

FIGURE 1 Experimental set-up for the generation, monochromatization and detection of the XUV light. L, 35-cm lens; SL, slits; TG, toroidal grating; SD, sine-drive rotation system; TP, turbomolecular pumps; B, baffles for stopping the diffused light; D, AXUV-Al or MCP detector

with an exit pinhole. In all the above geometries the laser beam was focused via a 35-cm focal length lens into the gas. The beam waist at the focus has been estimated to be ∼40 μm. From the evaluation of the different geometries, the gas laminar flow cell was found to be the most efficient one for the harmonic production. It is further found that, for this geometry, the distance between the laser focus and the cell pinhole plays a major role for the efficient XUV production. For example, for intensities up to about $2 \times 10^{14}\,\mathrm{W/cm^2}$ and for an argon-gas target, the generation is maximized when the focus of the laser is at the exit hole plane. The situation is different for higher intensities, where the ionization of the gas medium is strong. Laser defocusing due to propagation in an ionized medium makes the emission of lower wavelengths stronger when the laser focus is a few millimeters after the exit pinhole. Indeed refraction induces self-defocusing of the laser [44], bringing the actual intensity in the medium down to the ionization saturation level [45]. This process limits the effective intensity to the proper range suited for high-harmonic generation. The quasi-static cell arrangement is shown in Fig. 1. It has some similarity to previous set-ups, interfacing a gas cell with a vacuum chamber [46], but the propagation and XUV-production details are very dissimilar in the two cases, as in the previous set-up the main feature is waveguiding of the beam in a few-cm-long capillary, which is entirely missing in the present arrangement.

2.2 *Toroidal grating monochromator (TGM)*

The monochromator (Fig. 1) consists of an entrance pinhole and arm, the toroidal grating housing and its rotation system, and the exit arm and slit. The entrance pinhole is the exit pinhole of the quasi-static cell described in Sect 2.1. The length of the entrance arm is adjustable (under vacuum conditions) with micrometric resolution in a range of 10 mm and its central value is $l_\mathrm{A} = 319.93$ mm. The length of the exit arm is adjustable (under vacuum conditions) with micrometric resolution in a range of 30 mm and its central value is $l_\mathrm{B} = 319.50$ mm. The entrance and the exit arms form a fixed angle of 142°. Wavelength tuning is achieved by rotating the grating about the axis that is perpendicular to both arms of the monochromator at their intersection. The toroidal grating has a line spacing $N = 550$ lines/mm, a meridional radius of curvature $R_1 = 1000$ mm and a sagittal radius of curvature $R_2 = 104.09$ mm, and its physical dimensions are 31 mm × 31 mm × 15 mm. The rotation step of the grating angle is 2×10^{-6} rad as defined by the 2-μm linear resolution of the sine-bar of the rotation arrangement. The resolution of the monochromator for the given geometry is 0.2 nm at $\lambda = 30$ nm. The long-wavelength limit of the TGM in the first diffraction order is 385.4 nm. In the following the dependence of the diffraction efficiency of the grating as a function of the wavelength and its focusing properties as given by the manufacturer have been used.

2.3 *Detection and calibration systems*

For wavelengths lower than 40 nm, Absolute Extreme Ultraviolet (AXUV) Al-coated (100-nm coating film) Si diodes have been used for calibration purposes. These diodes have been specified by National Institute of Standards and Technology (NIST) as transfer standards in the 5-nm to 250-nm wavelength range. The diodes are passivated and thus long-term-stabilized with respect to their calibrated performance. When these diodes are exposed to photons of energy greater than 1.12 eV (wavelength less than 1100 nm), electron–hole pairs (carriers) are created. The device quantum efficiency (electrons seen by an external circuit per incident photon) is much larger than unity, and increases linearly with photon energy. Once the calibration with the AXUV diodes has been completed, a chevron-type multi-channel plate (MCP) detector has been used for the measurement of spectral regions in which the diodes are blind. The MCP detector is calibrated by recording spectral regions that have been measured with the AXUV diodes under the same experimental conditions. Calibration is extended to all other wavelength regions of interest is through the known MCP response as a function of the wavelength. The resulting calibration curve is shown in Fig. 2.

3 Experimental method – results

The experimental apparatus is shown in Fig. 1. The Ti:sapphire laser beam apertured at 1 cm is focused via a 35-cm focal length lens at the 50-μm exit pinhole of a noble-

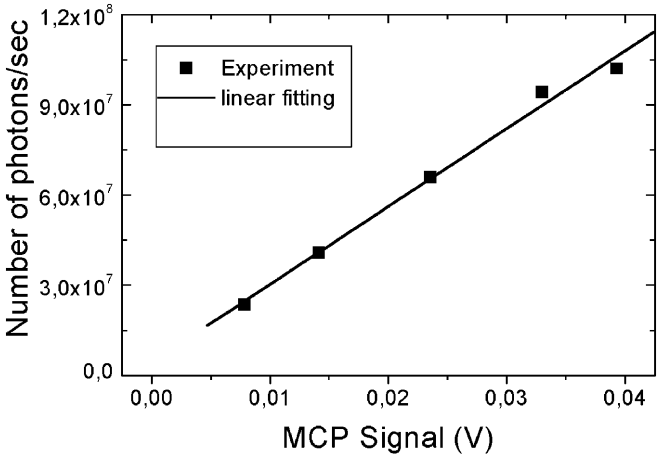

FIGURE 2 Calibration curve for the MCP detector

gas laminar flow cell which is kept at constant pressure. The laser pulse peak intensity at the focus was ranging between 10^{14} and 10^{15} W/cm^2 in the different runs. The laser beam co-propagating with the harmonics and the plasma emission are impinging on the toroidal grating. After monochromatization at the grating the XUV light is detected at the output of the monochromator. The maximum gas pressure in the first cell can be as high as 100 mbar while maintaining the pressure in the rest of the system below 10^{-5} mbar, through turbomolecular pump differential pumping. The MCP and AXUV diode signals are monitored through a lock-in amplifier locked at the laser repetition rate. The signal is stored as a function of the wavelength in a PC. A typical spectrum obtained with Kr as a target gas and detected by the AXUV-Al detector is shown in Fig. 3. The laser intensity reads about 5×10^{14} W/cm^2. The decrease of the signal above 32 nm is attributed to the 100-nm Al-film absorption and to the absorption of the krypton target gas itself.

The XUV harmonic emission from krypton and argon has been investigated for different intensity, pressure and focusing parameters as described below. Figure 4 illustrates the line-integrated XUV photon number per second, at the detection area, measured for various laser input intensities at 20-mbar Kr pressure. The results show that the dominant harmonic

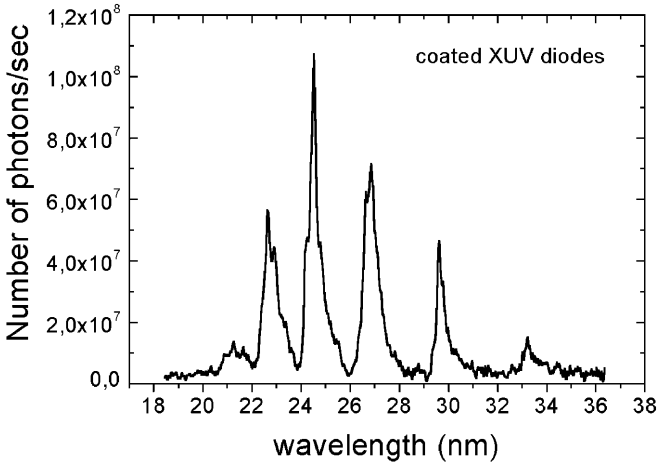

FIGURE 3 Typical spectrum obtained with the AXUV-Al diodes. The target was Kr (20 mbar) and the laser intensity 5×10^{14} W/cm^2

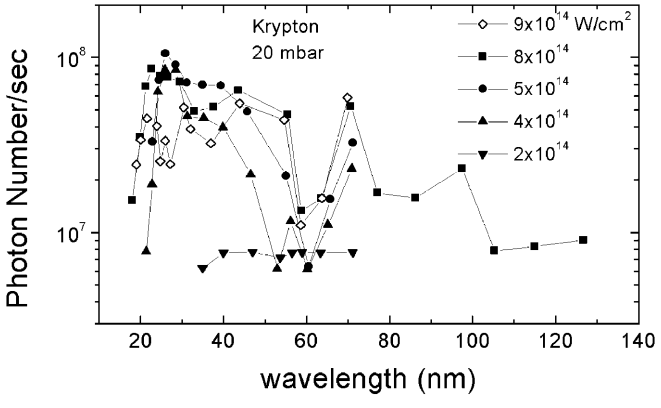

FIGURE 4 Line-integrated photon number per second as a function of wavelength and for various laser intensities for 20-mbar Kr-filled quasi-static cell. The focus is at the exit pinhole

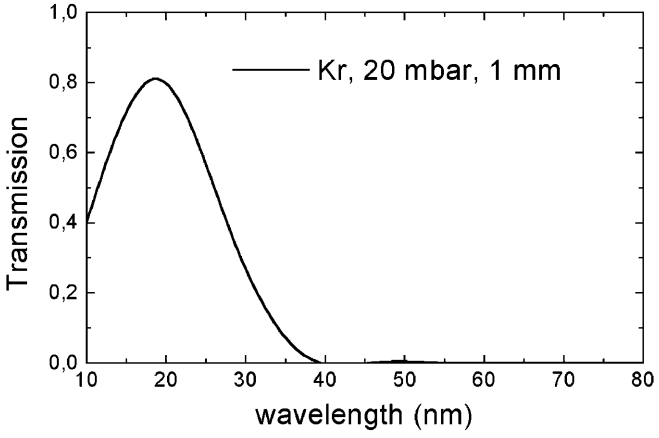

FIGURE 5 Calculated absorption of XUV light from 1-mm long neutral Kr medium

emission is in the range of 22–40 nm yielding approximately 10^8 photons/s. We observe up to the 39th harmonic down-shifted to ∼18 nm, which is much higher than that predicted by IP+3.2Up (IP is the ionization potential and Up is the ponderomotive energy calculated at barrier-suppressed ionization (BSI) intensity, 1.5×10^{14} W/cm^2 for Kr), which can be attributed to non-adiabatic behavior of the system [4]. The lower efficiency of the harmonic emission above 40 nm can be attributed both to the high reabsorption by the Kr gas in this area and to the lower diffraction efficiency of the gold grating. The abrupt decrease of the XUV light below 20 nm is attributed to the low diffraction efficiency of the grating. An estimation of Kr reabsorption is made by calculating its transmission as a function of the wavelength for 20-mbar Kr pressure and gas lengths of 1 mm as shown in Fig. 5. Figure 4 shows that the highest harmonic conversion efficiency is not necessarily achieved at the highest laser intensity. For some wavelength regions XUV generation becomes maximum at intermediate laser intensities. Thus for the harmonics located between 27 and 45 nm, maximum XUV generation is achieved at 5×10^{14} W/cm^2. For harmonics around 70 nm the maximum of XUV generation is at the maximum used laser intensity of 9×10^{14} W/cm^2. This behavior can be generally understood as follows: for intensities of the driving laser pulse higher than the ionization saturation intensity of the non-linear medium, a large number of charges are rapidly accumulated along the laser beam propagation volume, which results in a strong self-defocusing of the fundamental beam.

Spectroscopically resolved detailed characteristics of the emission are depicted in Fig. 6. Each of these spectra is normalized at its maximum value. Keeping the Kr pressure constant and varying the laser peak intensity from 4 to 9 times 10^{14} W/cm^2, several interesting phenomena can be observed. The first pronounced effect is the broadening of the harmonic lines with laser intensity. At the highest intensities used in the region around 25 nm the individual harmonics cannot be resolved at the present settings. Another observed effect is the blue shift of the harmonics. For the higher harmonics this shift approaches a $\Delta\lambda$ of about 5 nm, which is larger than the spacing between two subsequent harmonics. Furthermore, at the highest intensities used, the harmonics exhibit an irregular oscillatory spectral profile. The spectral envelope exhibits two

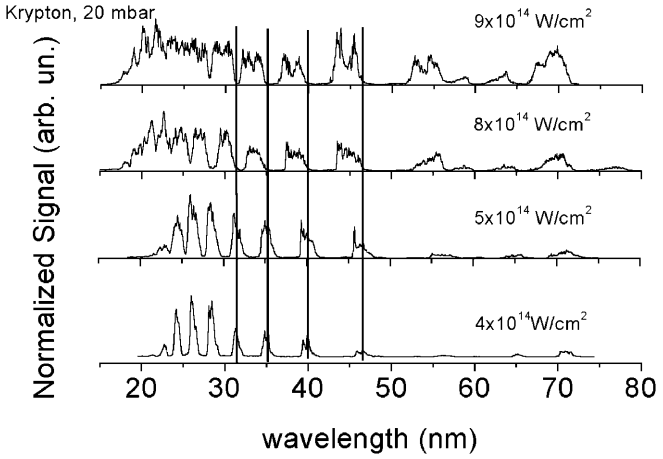

FIGURE 6 Normalized high-harmonic spectra obtained from 20-mbar Kr-filled quasi-static cell for various laser intensities. The focus is at the exit pinhole. The horizontal lines are for helping the eye to observe the blue shifting of the harmonics

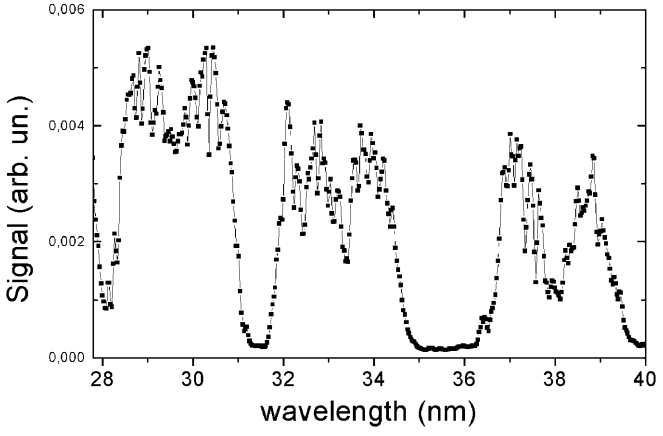

FIGURE 7 Details of the spectrum of Fig. 6 with the highest laser intensity (9×10^{14} W/cm^2)

main peaks per harmonic. Each of these peaks contains several spectral oscillations as shown in Fig. 7.

When the driving laser intensity is increased above the ionization saturation intensity of the non-linear medium, such a splitting has been very recently observed in Ar by Wang et al. [30]. These authors have attributed this effect to the rapid ionization of the medium, which induces strongly time-dependent refractive indices imparting a strong chirp to the propagating harmonics. The same effect has been previously theoretically predicted [26, 28] and attributed to the intensity-dependent dipole phase that gives rise to different blue shifts for different electron trajectories, thus leading to the splitting of the harmonic spectrum. The two peaks are formed by the two primary electron trajectories; the short and the long one [47–49].

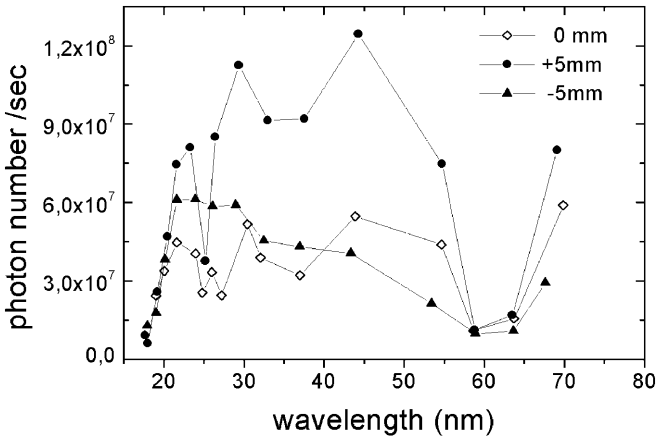

FIGURE 8 Line-integrated photon number per second as a function of wavelength for 20-mbar Kr-filled quasi-static cell and various focus positions with respect to the exit pinhole of the quasi-static cell. The laser intensity was 9×10^{14} W/cm^2

Further, the XUV generation has been examined as a function of the laser focus position with respect to the exit pinhole of the quasi-static gas cell. The focus has been moved by 5 mm in front of and behind the pinhole, in order to examine the role of propagation of high harmonics and the length of the generating medium. The results are shown in Fig. 8. When the focus is 5 mm behind the pinhole, there is an increase by more than a factor of two of the harmonic emission in the wavelength region between 25–50 nm. This can be attributed to the lower reabsorption of radiation because of the shorter propagation length in the medium. The emission spectra for various laser

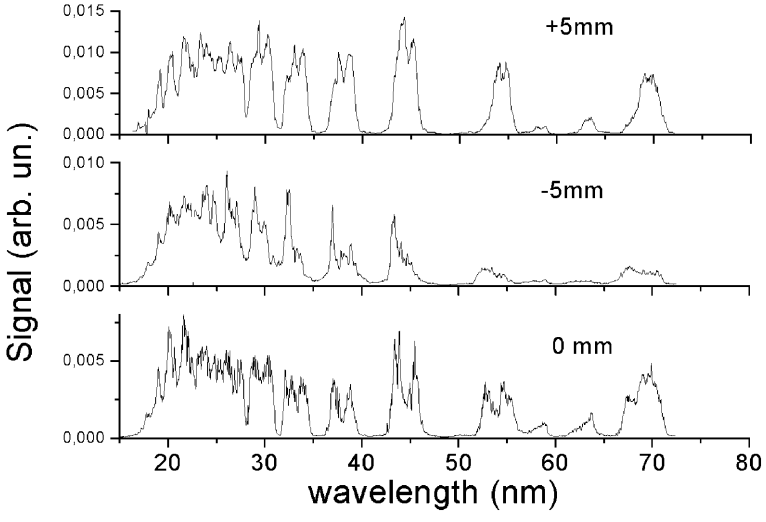

FIGURE 9 The corresponding normalized spectra for the laser focus positions of Fig. 8

focus conditions are shown in Fig. 9. The spectra of Fig. 9 show that the double peaking is present also when the focus position is 5 mm behind the pinhole, but the spectral profile is smoother in this case. The spectrum recorded with the beam focused 5 mm in front of the pinhole depicts asymmetric harmonic peaks.

This complex spatial behavior can be attributed to the existence of the two quantum paths described previously. As shown by Antoine et al. [36] and Salières et al. [50], the phase-matching conditions are different for the two paths, so that one remains phase-matched in a given focusing geometry, while the second is partially suppressed. As shown by Kim et al. [29], the shorter path is almost immune to laser intensity variations, so it experiences limited spectral broadening and shifting effects. The longer path in contrast displays strong phase variations with intensity, translating into a blue shift or blue broadening on the rising edge of the pulse, and therefore into an asymmetric harmonic profile.

Such an effect is observed in the present measurements and is shown in the second spectrum of Fig. 9. In this experiment the remaining trajectory seems to be the longer one, since the low photon energy sub-peak is the one that is strongly suppressed. The oscillatory features experimentally observed for the first time in the harmonic frequency profiles, when the laser beam is focused at the pinhole (Fig. 9), appear also in the theoretical spectra by Kim et al. [29]. We suggest the following explanation: assuming a Gaussian temporal profile $e^{-(t/T)^2}$, the frequency shift of the harmonic is

$$\Delta\omega = -2a\frac{t}{T^2}e^{-(t/T)^2}. \quad (1)$$

The $\Delta\omega$ reaches a maximum at the inflection point of the leading edge; therefore, any frequency shift lower than the maximum one will be obtained twice, once before the inflection point, and once after. This dual emission in the time domain will translate into oscillations in the spectral domain.

Further measurements have been performed using Ar gas as non-linear medium. The line-integrated photon number per second for each line is shown in Fig. 10. In contrast with the Kr case, the plateau extension remains below the value given

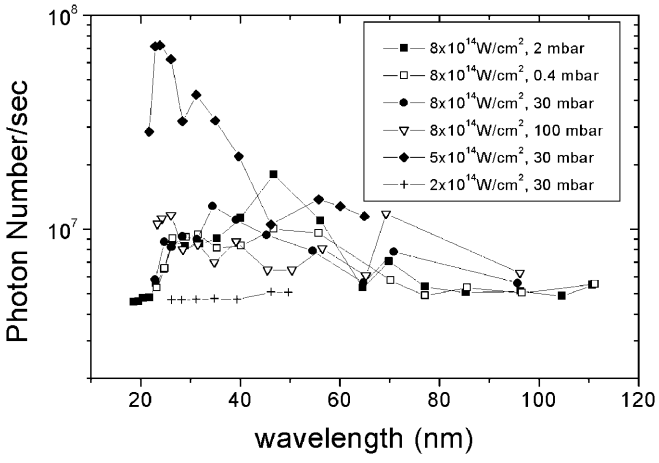

FIGURE 10 Line-integrated photon number per second as a function of wavelength and for various laser intensities and pressures of Ar-filled quasi-static cell. The focus is at the exit pinhole

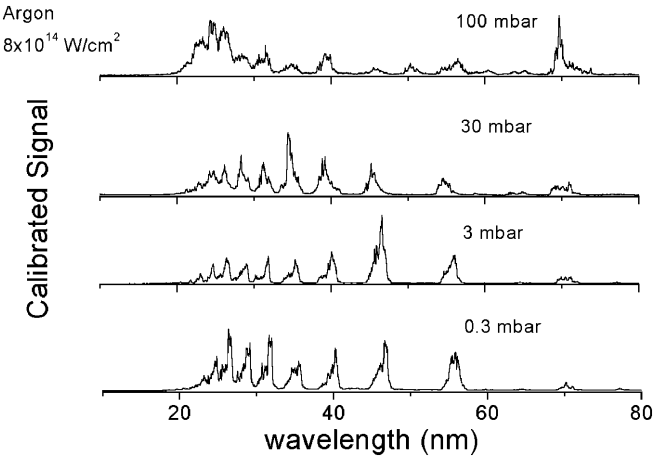

FIGURE 11 Normalized spectra obtained from various pressures of Ar-filled quasi-static cell while keeping constant the laser intensity (8×10^{14} W/cm^2). The focus is at the exit pinhole

by the IP + 3.2Up law at BSI intensity. From the spectra it is apparent that the harmonic generation in Ar is less efficient as compared to the generation in Kr, at least for the plateau harmonics that we study here. The maximum photon number per second measured reads $(1-2)\times 10^7$. On the other hand, the XUV efficiency in the wavelength range between 20–40 nm increases by a factor of five for a specific intensity and Ar pressure (5×10^{14} W/cm^2, 30 mbar). This may be attributed to good phase-matching conditions for these specific pressure and intensity values. The dependence of the XUV yield on the target pressure, measured at constant laser intensity, is illustrated in Fig. 11. The laser intensity is 8×10^{14} W/cm^2, while the focus of the laser beam is at the exit pinhole of the XUV-generating cell. The Ar pressure is varied from 0.3 mbar to 100 mbar. In every spectrum of Fig. 10, the signal is normalized to its maximum value. From Fig. 11 it is clear that there is no significant broadening of harmonic emission due to the increase of the Ar pressure, expect for the case of 100 mbar (maximum pressure used) in the higher-harmonic region. A small blue shifting of the harmonic peaks has been observed but no clear double peaks are present, as in the case of Kr. This is compatible with the fact that the ionization saturation intensity forAr is higher than that for Kr.

Attempting an overall assessment of the source we conclude that its performance with respect to the photon numbers in combination with the covered spectral area is comparable to other similar existing sources [9, 51]. Considering its compactness, transportability and versatility its performance can be deemed satisfactory. It should be noted again here that all given photon number values are measured at the exit slit of the source and not at the generation area. It should be further pointed out that the performance of the source has not been optimized for specific wavelength regions through phase-matching or phase-control approaches. It is an 'all purpose' performance set-up, with a source operating in an extended wavelength region and with intermediate pumping requirements. The source has not been tested under conditions optimizing the production of one harmonic. In such a case it is known that the conversion efficiency of the source may be increased substantially [12, 52].

4 Extension and possible uses of the XUV source

As mentioned above, in the wavelength region around 30 nm (region around the 27th harmonic) the source delivers 10^8 photons/s (measured), in pulses of less than 1.6-ps duration, as estimated using the grating characteristics and the analysis by Villoresi [53]. For a focus spot of 0.01 mm^2, these parameters result in an estimated focused XUV intensity of about 5×10^6 W/cm^2. The intensity of certain harmonics can be further increased through optimized tailoring of the phase front of the laser pulses using a spatial light modulator. In addition to representing sufficient flux for time-resolved linear XUV spectroscopy, such intensities keep open the perspective of inducing a non-linear process with a higher harmonic, but of course this remains a tedious task to implement.

Other possible applications of the source would be the study of molecular dynamics. To mention some examples, the decay time of C60 when excited to a plasmon resonance near 20 eV could be extracted. Using ion/electron imaging detection combined with the XUV source presented here, the dynamics of molecular photodissociation of interesting molecules (e.g. ozone) by simultaneous time-, energy- and angular-resolved experiments can be investigated.

ACKNOWLEDGEMENTS This work is supported by the ULF facility (Contract No. ERBFMGECT 950 021), the FIRE program (Contract No. ERBFMGECT 980 095) and ATTO (Contract No. HPRN-2000-00133). The test of the source has been carried out in the European Laser Facility at Laboratoire d'Optique Appliquée (LOA) at Palaiseau, Paris. We thank Andre Mysyrowicz for his help with the coordination within the FIRE project. We would also like to thank Argirios Kasiotakis and Genevieve Mullot for skillful technical assistance. N.A.P. and D.C. would like to thank the people at LOA for their hospitality. E.G. acknowledges the support by EPEAK national graduate program (Greek ministry of education).

REFERENCES

1 H. Eichmann, S. Meyer, K. Riepl, C. Momma, B. Wellegehausen: Phys. Rev. A **50**, R2834 (1994)
2 M.B. Gaarde, P. Antoine, A. Persson, B. Carré, A. L'Huillier, C.-G. Wahlström: J. Phys. B: At. Mol. Opt. Phys. **29**, L163 (1996)
3 A. Nazarkin, G. Korn, O. Kittelmann, J. Ringling, I.V. Hertel: Phys. Rev. A **56**, 671 (1997)
4 J. Zhou, J. Peatross, M.M. Murnane, H.C. Kapteyn: Phys. Rev. Lett. **76**, 752 (1996)
5 M. Schnurer, Ch. Spielmann, P. Wobrauschek, C. Streli, N.H. Burnett, C. Kan, K. Ferencz, R. Koppitsch, Z. Cheng, T. Brabec, F. Krausz: Phys. Rev. Lett. **80**, 3236 (1998)
6 C. Kan, N.H. Burnett, C.E. Capjack, R. Rankin: Phys. Rev. Lett. **79**, 2971 (1997)
7 Z. Chang, A. Rundquist, H. Wang, M.M. Murnane, H.C. Kapteyn: Phys. Rev. Lett. **79**, 2967 (1997)
8 A. de Bohan, P. Antoine, D.B. Milosevic, B. Piraux: Phys. Rev. Lett. **81**, 1837 (1998)
9 L. Roos, E. Constant, E. Mével, P. Balcou, D. Descamps, M.B. Gaarde, A. Valette, R. Haroutunian, A. L'Huillier: Phys. Rev. A **60**, 5010 (1999)
10 U. Andiel, G.D. Tsakiris, E. Cormier, K. Witte: Europhys. Lett. **47**, 42 (1999)
11 A. Rundquist, C.G. Durfee III, Z. Chang, C. Herne, S. Backus, M.M. Murnane, H.C. Kapteyn: Science **280**, 1412 (1998)
12 Y. Tamaki, J. Itatani, Y. Nagata, M. Obara, K. Midorikawa: Phys. Rev. Lett. **82**, 1422 (1999)
13 H.R. Lange, A. Chiron, J.-F. Ripoche, A. Mysyrowicz, P. Breger, P. Agostini: Phys. Rev. Lett. **81**, 1611 (1998)
14 Y. Kobayashi, T. Sekikawa, Y. Nabekawa, S. Watanabe: Opt. Lett. **23**, 64 (1998)
15 T. Sekikawa, T. Ohno, T. Yamazaki, Y. Nabekawa, S. Watanabe: Phys. Rev. Lett. **83**, 2564 (1999)
16 J. Norin: ATTO Network Meet., Paris, 25–27 January 2001
17 T. Ditmire, J.W.G. Tisch, E.T. Gumbrell, R.A. Smith, D.D. Meyerhofer, M.H.R. Hutchinson: Appl. Phys. B **65**, 313 (1997)
18 L. Le Déroff, P. Salières, B. Carré, D. Joyeux, D. Phalippou: Phys. Rev. A 61, 043 802 (2000)
19 M. Bellini, C. Lyngå, A. Tozzi, M.B. Gaarde, T.W. Hänsch, A. L'Huillier, C.-G. Wahlström: Phys. Rev. Lett. **81**, 297 (1998)
20 P. Salières, L. Le Déroff, T. Auguste, P. Monot, P. d'Oliveira, D. Campo, J.-F. Hergott, H. Merdji, B. Carré: Phys. Rev. Lett. **83**, 5483 (1999)
21 P. Antoine, B. Carré, A. L'Huillier, M. Lewenstein: Phys. Rev. A **55**, 1314 (1997); P. Antoine, A. L'Huillier, M. Lewenstein, P. Salières, B. Carré: Phys. Rev. A **53**, 1725 (1996)
22 F.A. Weihe, S.K. Dutta, G. Korn, D. Du, P.H. Bucksbaum, P.L. Shkolnikov: Phys. Rev. A **51**, R3433 (1995)
23 E. Constant, V.D. Taranukhin, A. Stolow, P.B. Corkum: Phys. Rev. A **56**, 3870 (1997)
24 C. Altucci, C. Delfin, L. Roos, M.B. Gaarde, A. L'Huillier, I. Mercer, T. Starczewski, C.-G. Wahlström: Phys. Rev. A **58**, 3934 (1998)
25 P. Salières, T. Ditmire, M.D. Perry, A. L'Huillier, M. Lewenstein: J. Phys. B: At. Mol. Opt. Phys. **29**, 4771 (1996)
26 C. Kan, C.E. Capjack, R. Rankin, N.H. Burnett: Phys. Rev. A **52**, R4336 (1995)
27 C. Altucci, R. Bruzzese, C. de Lisio, M. Nisoli, S. Stagira, S. De Silvestri, O. Svelto, A. Boscolo, P. Ceccherini, L. Poletto, G. Tondello, P. Villoresi: Phys. Rev. A **61**, 021801(R) (1999)
28 H.J. Shin, D.G. Lee, Y.H. Cha, K.H. Hong, C.H. Nam: Phys. Rev. Lett. **83**, 2544 (1999)
29 J.-H. Kim, H.J. Shin, D.G. Lee, C.H. Nam: Phys. Rev. A **62**, 055 402 (2000)
30 Y. Wang, Y. Liu, X. Yang, Z. Xu: Phys. Rev. A **62**, 063 806 (2000)
31 T.W. Hansch: Opt. Commun. **80**, 71 (1990)
32 G. Farkas, Cs. Toth: Phys. Lett. A **168**, 447 (1992)
33 S.E. Harris, J.J. Macklin, T.W. Hansch: Opt. Commun. **100**, 487 (1993)
34 P.B. Corkum, N.H. Burnett, M.Y. Ivanov: Opt. Lett. **19**, 1870 (1994)
35 M. Protopapas, D.G. Lappas, C.H. Keitel, P.L. Knight: Phys. Rev. A **53**, R2933 (1996)
36 P. Antoine, A. L'Huillier, M. Lewenstein: Phys. Rev. Lett. **77**, 1234 (1996)
37 I.P. Christov, M.M. Murnane, H.C. Kapteyn: Phys. Rev. Lett. **78**, 1251 (1997)
38 N.A. Papadogiannis, B. Witzel, C. Kalpouzos, D. Charalambidis: Phys. Rev. Lett. **83**, 4289 (1999)
39 E.S. Toma, H.G. Muller, P.M. Paul, P. Breger, M. Cheret, P. Agostini, C. Le Blanc, G. Mullot, G. Cheriaux: Phys. Rev. A **62**, 061801(R) (2000)
40 M. Drescher, M. Hentschel, R. Kienberger, G. Tempea, C. Spielmann, G.A. Reider, P.B. Corkum, F. Krausz: Science **291**, 1923 (2001)
41 P.M. Paul, E.S. Toma, P. Breger, G. Mullot, F. Augé, Ph. Balcou, H.G. Muller, P. Agostini: Science **292**, 1689 (2001)
42 S. Cavalieri, R. Eramo: Phys. Rev. A **58**, R4263 (1998)
43 M. Gisselbrecht, D. Descamps, C. Lyngå, A. L'Huillier, C.-G. Wahlström, M. Meyer: Phys. Rev. Lett. **82**, 4607 (1999)
44 P. Monot, T. Auguste, L.A. Lompre, G. Mainfray, C. Manus: J. Opt. Soc. Am. B **9**, 1579 (1992)
45 E.E. Fill: J. Opt. Soc. Am. B **11**, 2241 (1994)
46 M. Schnurer, Z. Cheng, S. Sartania, M. Hentschel, G. Tempea, T. Brabec, F. Krausz: Appl. Phys. B **67**, 263 (1998)
47 P.B. Corkum: Phys. Rev. Lett. **71**, 1994 (1993)
48 K.J. Schafer, B. Yang, L.F. DiMauro, K.C. Kulander: Phys. Rev. Lett. **70**, 1599 (1993)
49 M. Lewenstein, Ph. Balcou, M.Yu. Ivanov, A. L' Huillier, P.B. Corkum: Phys. Rev. A **49**, 2117 (1994)
50 P. Salières, B. Carré, L. Le Déroff, F. Grasbon, G.G. Paulus, H. Walther, R. Kopold, W. Becker, D.B. Miloevi, A. Sanpera, M. Lewenstein: Science **292**, 902 (2001)
51 C. de Lisio, C. Altucci, R. Bruzzese, F. De Filippo, S. Solimeno, M. Bellini, P. Foggi: Appl. Phys. B **64**, 323 (1997)
52 E. Constant, D. Garzella, P. Breger, E. Mével, Ch. Dorrer, C. Le Blanc, F. Salin, P. Agostini: Phys. Rev. Lett. **82**, 1668 (1999)
53 P. Villoresi: Appl. Opt. **38**, 6040 (1999)